Asymmetric Line Shapes for Medium Energy H and He Ions Undergoing a Large-angle Collision

M. Hazama[1], Y. Kitsudo[1], T. Nishimura[1], Y. Hoshino[2], P.L. Grande[3], G. Schiwietz[4], and Y. Kido[1]

Abstract

Asymmetric line shapes for medium energy H and He ions backscattered from topmost adatoms such as Si(111)-$\sqrt{3}\times\sqrt{3}$-Sb and Ni(111)-2×2-O are measured by a toroidal electrostatic analyzer with an excellent energy resolution. The spectra exhibit a pronounced asymmetric nature and are well fitted by an exponentially modified Gaussian profile. It is found that the non-perturbative coupled-channel calculations reproduce well the observed asymmetric line shapes for He^+ impact on different materials, although slightly overestimate the asymmetry for H^+ impact on Au. On the other hand, the CasP 3.2 program (involving additional approximations) gives large underestimates for He ions and overestimates for H ions. This problem has been partially solved by modifying the order of the implementation of the shell corrections and higher-order effects in the CasP model.

[1] *Department of Physics, Ritsumeikan University, Kusatsu, Shiga-ken 525-8577, Japan*

[2] *Department of Information Science, Kanagawa University, Hiratsuka, Kanagawa 259-1293, Japan*

[3] *Instituto de Física da Universidade Federal do Rio Grande do Sul, Avenida Bento Gonçalves 9500, 91501-970 Porto Alegre, Brazil*

4 Hahn-Meitner-Institut, Abteilung SF4 Glienicker Str. 100, 14109 Berlin, Germany

1. Introduction

Medium energy ion scattering spectroscopy (MEIS) provides a powerful tool to clarify quantitatively surface and interfaces structures[1-6] and lattice dynamics near surfaces regions[7-9] in a layer-by-layer fashion. In the high-resolution MEIS analysis, however, we meet fine structures making the analysis complicated such as non-equilibrium charge state distributions[10, 11] and asymmetric profiles of backscattered ions[12-14], which are not visible in conventional ion scattering analysis. For reliable data analysis, it is strongly required to understand systematically the above phenomena and to derive some expressions analytically. Concerning the asymmetric line shapes, there are some experimental and theoretical studies reported so far for medium energy H^+ impact[15-17]. From a theoretical viewpoint, it is essential to calculate the energy-loss distribution under a single large-angle collision condition. For individual electrons, a coupled channel formulation allows for numerical calculations even for strong electrostatic perturbations[18]. Such calculations agree quite well with the recent experimental data for 100 keV H^+ impact[15-17]. Unfortunately, these calculations consume very long computing time. To overcome this problem, a simplified method to estimate the energy-loss distribution based on the unitary convolution approximation was proposed[19]. This model is implemented in the CasP program[20], where the asymmetric line shape is expressed by exponentially modified Gaussian (EMG) profile.

In this study, high-resolution MEIS spectra are measured for H^+ and He^+ ions backscattered from topmost atoms under a nearly single collision condition and compared to different theoretical calculations. Previous comparisons[15-17] have been performed for H projectiles only in the perturbative regime at 100 keV/amu ($Z/v = 0.5$, Z being the projectile nuclear charge and v the projectile speed, in atomic units). Z/v is about 2 in the present case (for He ions), where the projectile is not bare and capture and loss come additionally into play. Here, different higher-order effects will be very important and experimental results are needed to test theoretical calculations in this non-perturbative regime.

2. Experiment

The experimental energy-loss spectra are obtained from a toroidal electrostatic analyzer (ESA) with an excellent relative energy resolution ($\Delta E / E$) of $1.3\pm0.1\times10^{-3}$ (FWHM, determined from the present experimental data assuming a Gaussian

transmission function). The use of gas targets does not easily allow observing backscattering spectra under a single collision condition because of extremely small scattering yield. This is due to constraint that the gas target should be dilute enough to suppress multiple scattering and to keep an ultra-high vacuum (UHV). For small-angle forward scattering (scattering angle: a few mrad), however, Auth and Winter[21] observed beautiful line shapes involving elastic and inelastic components using medium energy proton beams and had good agreement between their observation and the first-order perturbation[22] in the mean energy loss and straggling. In order to view the line shapes for a large-angle scattering, it is essential to prepare characteristic surfaces such as adatoms/substrate structures. We prepared Si(111)-$\sqrt{3}\times\sqrt{3}$-Sb, Ni(111)-2×2-O, and Au(0.25-0.45 ML)/Ni(111) surfaces and measured *in situ* the MEIS spectra. How to form the Ni(111)-2×2-O and Si(111)-$\sqrt{3}\times\sqrt{3}$-Sb is referred to the literature[13,23]. The chemisorbed O atoms take an upper position of 1.2 Å from the top Ni(111) plane[24] and the distance between the Sb layer and the first Si(111) plane is estimated to be 2.63 Å for the $\sqrt{3}\times\sqrt{3}$-Sb surface[25]. We deposited Au (0.25 -0.45 ML) on Ni(111) at room temperature using a Knudsen cell at a rate of 0.2 ML/min (1 ML = 1.86×10^{15} atoms/cm^2: areal density of Ni(111)). Figures 1(a), (b), (c), and (d) indicate the RHEED (reflection high-energy electron diffraction) patterns taken for Ni(111), Ni(111)-2×2-O, Au(0.45 ML)/Ni(111), and Si(111)-$\sqrt{3}\times\sqrt{3}$-Sb surfaces, respectively. The RHEED pattern observed for Au/Ni(111) shows growth of two-dimensional (2D) Au(111) islands with the bulk Au-Au bond length of 2.88 Å (bulk Ni-Ni bond length is 2.49 Å).

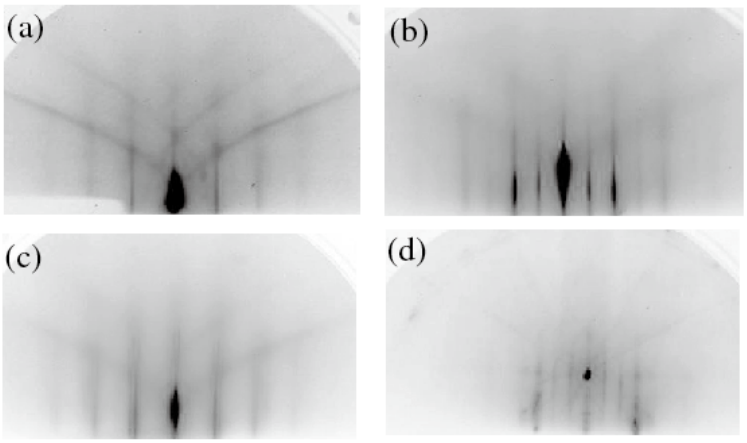

FIG. 1. RHEED patterns taken for (a) Ni(111), (b) Ni(111)-2×2-O, (c) (0.45 ML)/Ni(111), and (d) Si(111)-$\sqrt{3}\times\sqrt{3}$-Sb surfaces.

3. Results and Discussion

The asymmetric line shapes for H^+ and He^+ ions undergoing a single atomic collision are basically derived from a semi-classical approximation[26], shell-by-shell and independent-electron model. Based on first-order perturbation theory, Kabachnik calculated impact-parameter (b) dependent electronic energy loss $Q(b)$ assuming a straight ion trajectory[22]. Using the much more reliable coupled-channel method[18,27], we solve the following time-dependent Schrödinger equation for one active electron,

$$i\hbar \frac{\partial \Psi_e(t)}{\partial t} = \hat{H}_e(t)\Psi_e(t), \tag{1}$$

with

$$\hat{H}_e(t) = V_{pe}(\vec{R}(t)-\vec{r}) + \hat{H}_{te}(\vec{r}) = -\frac{Z_p e^2}{|\vec{R}(t)-\vec{r}|} + \hat{H}_{te}(\vec{r}),$$
$$\hat{H}_{te} = -e\,V_t(\vec{r}) + T_e(\vec{r}_e) \tag{2}$$

where $\vec{R}(t)$, $\vec{r}$ and $\vec{r}_e$ denote the inter-nuclear distance, position vectors of the active electron scaled from a target nucleus and from the center-of-mass of the collision system, respectively. $V_t(\vec{r})$ and $T_e(\vec{r}_e)$ express a Hartree-Fock-Slater potential for the active electron[28] and kinetic energy of the active electron in the center-of-mass frame, $-e$ $(e>0)$ the electronic charge and $Z_p e$ the projectile charge. In the case of He^+ impact, the interaction potential is given by

$$V_{pe}(\vec{R}(t)-\vec{r}) = -\frac{Z_p e^2}{|\vec{R}(t)-\vec{r}|} + \int d\vec{r}\,' \frac{|\Phi_{1s}(\vec{r}\,')|^2}{|\vec{R}(t)-\vec{r}-\vec{r}\,'|} e^2, \tag{3}$$

where Φ_{1s} is the wave function of the 1s state of He^+. The classical projectile trajectory $\vec{R}(t)$ can be either determined in advance by solving the Newtonian equation, or simply replaced by a straight-line. Excitation and ionization probabilities are numerically calculated shell-by-shell allowing the contributions of transitions for about 500 discrete and continuum (wave-packet) states with orbital quantum numbers up to $l = 8$ and energies up to $2m_e v^2$ (m_e: electron mass, v: ion velocity), respectively.

The coupled channel calculation needs very long computing time and thus the application is limited to only a few selected collision systems. Grande and Schiwietz[19] synthesized the CasP 3.2 program, which is based on the unitary convolution approximation and uses a simplified method to calculate the impact-parameter

dependence of inelastic mean energy loss $Q(b)$. The energy-loss distribution is then obtained by using the model as proposed by Vickridge and Amsel[29] for resonant nuclear reactions and recently extended to MEIS[30]. The CasP 3.2 is now accessible via URL and widely utilized. It should be pointed out that this approach is based on an extension of first-order perturbation theory and thus it may break down abruptly at low projectile velocities.

Figures 2 (a) and (b) show the MEIS spectra observed for 100 keV H^+ ions and 120 keV He^+ ions, respectively incident along the [001]-axis of Ni(111) and backscattered from Au on top to 35.3° scaled from the surface normal. The observed MEIS spectra are well fitted by the exponentially modified Gaussian (EMG) shape proposed by Grande et al.[30], which is expressed by

$$f(\Delta E) = \frac{1}{2\sigma_0} exp\{-\frac{1}{2\sigma_0}(2\Delta E - \frac{\sigma^2}{\sigma_0})\}\{1 + erf(\frac{\Delta E - \sigma^2/\sigma_0}{\sqrt{2}\sigma})\}, \quad (4)$$

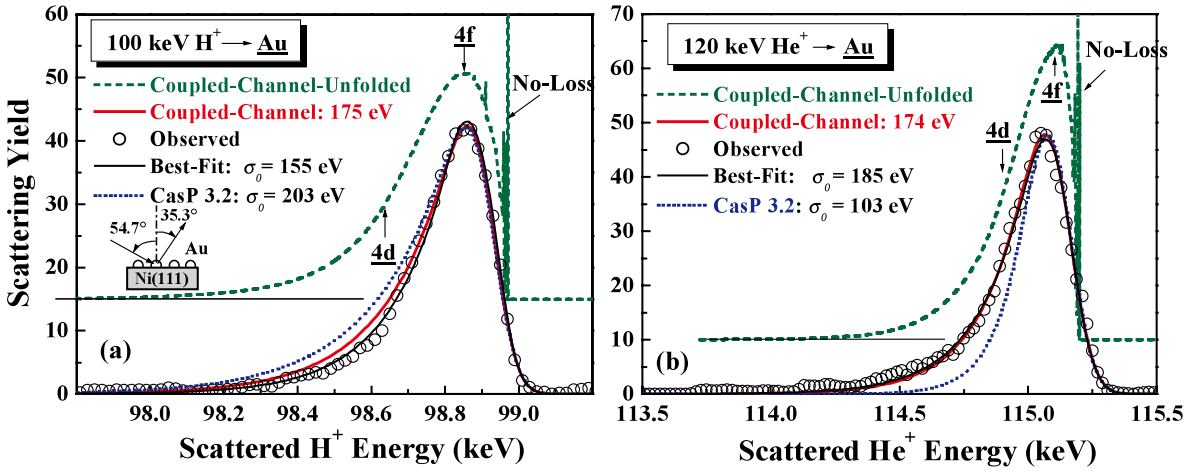

FIG. 2. MEIS spectra observed (circles) for (a) 100 keV H^+ and (b) 120 keV He^+ ions incident along the [001]-axis and backscattered from Au on top into the [110] direction of Ni(111). Black, red and blue solid and dotted curves denote respectively, the EMG line shapes best-fitted to the observed spectra (σ_0 = 155 eV for 100 keV H^+, σ_0 = 185 eV for 120 keV He^+), derived from coupled channel calculations (σ_0 = 175 eV for 100 keV H^+, σ_0 = 174 eV for 120 keV He^+), and from CasP 3.2 (σ_0 = 203 eV for 100 keV H^+, σ_0 = 103 eV for 120 keV He^+). The dashed curves (green) indicate the original inelastic energy-loss distributions of the coupled channel calculations before being convoluted with the instrumental function.

where *erf(x)* is an error function, σ experimental system resolution, and σ_0 quantifying an asymmetry induced by a large-angle collision. The best-fits are obtained assuming the σ_0 values of 155 eV for H^+ impact and of 185 eV for He^+ impact. For 120 keV He^+ ions backscattered from Au, the coupled channel calculation (b = 0, σ_0 = 174 eV) reproduces well the observed MEIS spectrum, while slightly overestimates for 100 keV H^+ impact on Au (b = 0, σ_0 = 175 eV). In the present coupled-channel calculations electrons in the sub-shells with binding energies below that of the 4d state are taken into account. The dashed curve (green) in each figure indicates the excitation-ionization probability obtained after convoluting all corresponding one-electron excitation-ionization probabilities with each other (not convoluted with the instrumental function). Thus, all multiple-reaction processes (e.g. double ionization) are included. Nevertheless, the main contribution comes from a

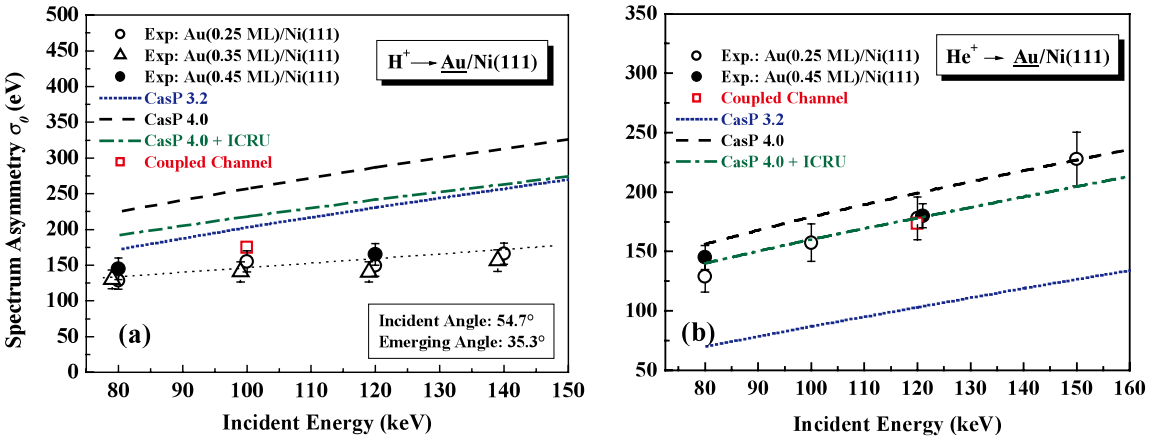

FIG. 3. Spectrum asymmetry σ_0 (circles and triangles) determined as a function of the incident energy for (a) H^+ and (b) He^+ impact on Au/Ni(111). Open square and curves denote coupled-channel and CasP calculations, respectively. (a) Black dotted line is drawn to guide the eyes.

single inner-shell ionization.

The energy dependence of the asymmetry σ_0 is shown in Figs. 3(a) and (b) for H^+ and He^+ ions backscattered from Au (0.25-0.5 ML) stacked on Ni(111). The σ_0 value increases gradually with increasing incident energy as predicted by theoretical calculations. For He^+ impact, the observed σ_0 values are much larger than the CasP 3.2 results, while significantly smaller than the CasP 3.2 data for H^+ impact.

The situation for He^+ impact on Au is quite the same as those for Ni(111)-2×2-O,

Ni(111), and Si(111)-$\sqrt{3}\times\sqrt{3}$-Sb. Figure 4 shows Z_2(target Z-number)-dependence of the spectrum asymmetry σ_0 for 120 keV He^+ incidence. The observed σ_0 values agree rather well with the coupled channel calculations. As can be also observed in Fig. 4, the CasP 3.2 data, give much smaller values than the observed ones. In fact, the description of σ_0 depends strongly on how accurate the inner-electrons (with binding energies close to the detector resolution) are treated. Since these electrons have orbital

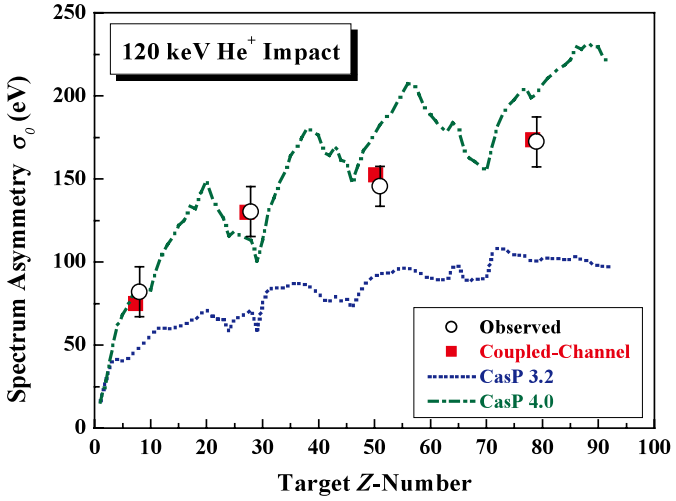

FIG. 4. Z_2-dependence of σ_0 determined experimentally (circles), from coupled–channel (squares), and CasP (curves) calculations.

velocities much larger than projectile one, the results will be sensitive to shell corrections (effect of electron motion) and the corresponding interplay with higher-order effects. We have modified the CasP program by exchanging the order of the higher-order effects and shell corrections. This has a minor effect for the valence electrons where most of the stopping power comes from. In addition we have added an estimate for the Barkas effect. This effect is important for close collisions as well as the long-ranged dipolar interactions. Since close encounters are reasonably well described by classical two-body collisions we make use of the Binary model[31] by Sigmund and Schinner by using the Barkas enhancement from this model as a multiplicative correction factor. No explicit solution has been included for the polarization due to long-ranged dipolar interactions. This new program version is called CasP 4.0.

The results of the new CasP version (CasP 4.0) for the asymmetry parameter σ_0 are shown in Figs. 3(a) and (b) as a function of the projectile energy. While the new results get slightly worse for H^+ projectiles, they are significantly better for He^+

projectiles. This comes from the interplay between higher-order effects (that are larger for He case) and the shell corrections. Now, differently from the CasP 3.2 data, the CasP

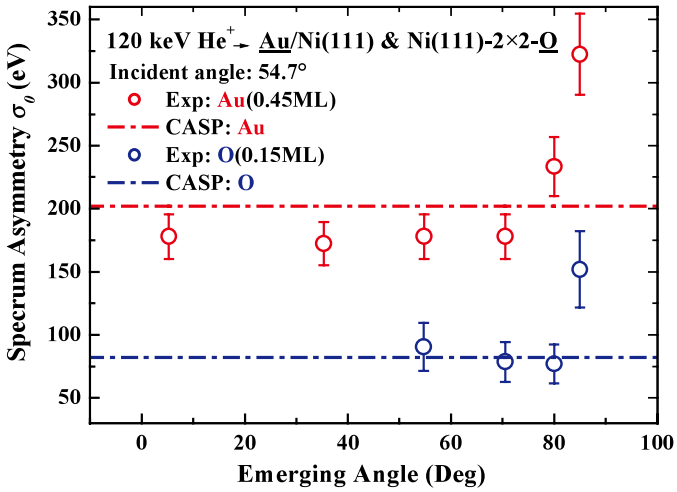

FIG. 5. σ_0 value as a function of emerging angle determined for 120 keV He^+ ions incident at 54.7° and backscattered from Au/Ni(111) and Ni(111)-2×2-O (red and blue circles). Dashed-dotted lines indicate new CasP calculations.

4.0 results overestimate the experimental data for both projectiles. Thus, the remaining disagreement can be consistently attributed either to general uncertainties of the model such as the shell corrections at low energies or to the simplified set of oscillator strengths used by the program as default. In fact, calculations using a more reliable set of oscillator strengths, as, e.g., the one from ref [32] (see dashed-dotted curves in Fig. 3) provide a much better overall agreement.

The adatoms/substrate structures except for Ni(111) used here satisfies almost single collision conditions. The [001] incidence and [110] emergence double-alignment geometry set for Ni(111) also provides nearly single-collision conditions for the scattering component from Ni. Figure 5 shows exit-angle dependence of the asymmetry σ_0 for 120 keV He^+ ions backscattered from Au and O on Ni(111). Here, the incident angle was fixed to 54.7° , corresponding to incidence along the [001]-axis of Ni(111). As clearly seen, the asymmetry (σ_0) is constant for emerging angles up to 70° for Au/Ni(111) and up to 80° for Ni(111)-2×2-O. At larger emerging angles, however, the σ_0 value dramatically increases owing to interaction with neighboring surface atoms. The emerging angle dependence of σ_0 certifies almost a single collision

condition for emerging angle below 70° for H^+ and He^+ impact, consistent with the CasP 4.0 results.

4. Summary

In summary, we measured the MEIS spectra for H^+ and He^+ ions backscattered from O, Ni, Sb, and Au atoms on top using Ni(111)-2×2-O, Si(111)-$\sqrt{3}\times\sqrt{3}$-Sb, and Au(0.25-0.45 ML) /Ni(111) surfaces, which allowed nearly single collision conditions. For Ni(111), double alignment geometry ([001]-incidence and [110]-emergence) also made it possible to measure the MEIS spectra for ions undergoing a nearly single collision. The observed MEIS spectra showed a pronounced asymmetric nature and are well fitted by an exponentially modified Gaussian (EMG) shape. The spectrum asymmetry σ_0 defining the EMG line shape calculated from the coupled-channel formulation agrees well with the observed one even in the cases where large perturbations take place, as for He^+ impact on Au. In contrast, the CasP 3.2 data show much smaller σ_0 values for He^+ impact on O, Ni, Sb, and Au, while significantly larger σ_0 values for H^+ impact on Au. The modification on how the shell corrections are implemented as well as the introduction of the Barkas effect in the CasP code largely improve the σ_0 values for He^+ impact. The remaining differences may partly be attributed to the somewhat oversimplified set of oscillator strengths used as default in the CasP program.

Acknowledgments

The authors would like to thank Dr. T. Okazawa for his help in carrying out the MEIS experiment. This work was partly supported by Japan Science and Technology Agency, JST, CREST.

References

1. J.F. van der Veen, Surf. Sci. Rep. **5**, 199 (1985).
2. J. Vrijmoeth, P.M. Zagwijn, J.W.M. Frenken, J.F. van der Veen, Phys. Rev. Lett. **67**, 1134 (1991).
3. K. Kimura, K. Nakajima, Y. Fujii, M. Mannami, Surf. Sci. **318**, 363 (1994).
4. P. Statiris, H.C. Lu, T. Gustafsson, Phys. Rev. Lett. **72**, 3574 (1994).
5. T. Nishimura, A. Ikeda, H. Namba and Y. Kido, Surf. Sci. **411**, L834 (1998).
6. P. Bailey, T.C.Q. Noakes, D.P. Woodruff, Surf. Sci. **426**, 358 (1999).
7. K.H. Chae, H.C. Lu, T. Gustafsson, Phys. Rev. **B 54**, 14082 (1996).
8. T. Okazawa, S. Ohno, Y. Hoshino, T. Nishimura, Y. Kido, Nucl. Instrum. and Methods **B 183**, 108 (2001).
9. T. Okazawa, T. Nishimura, and Y. Kido, Phys. Rev. **B 66**, 125402 (2002).
10. Y. Kido, T. Nishimura, and F. Fukumura, Phys. Rev. Lett. **82**, 3352 (1999).
11. Y. Kido, T. Nishimura, Y. Hoshino, E. Toyoda and T. Nakada, Phys. Rev **B 64**, 193403 (2001).
12. W.H. Schulte, H. Ebbing, H.W. Becker, M. Berheide, M. Buschmann, C. Rolfs, G.E. Mitchell, J.S. Schweitzer, J. Phys. **B 27**, 5271 (1994).
13. W.H. Schulte, B.W. Busch, E. Garfunkel, T. Gustafsson, G. Schiwietz, P.L. Grande, Nucl. Instrum. Methods **B 183**, 16 (2001).
14. Y. Kido, S. Semba, Y. Hoshino, Nucl. Instrum. Methods **B 219-220**, 599 (2004).
15. P.L. Grande, A. Hentz, G. Schiwietz, W.H. Schulte, B.W. Busch, D. Starodub, T. Gustafsson, Phys. Rev. **B 69**, 104112 (2004).
16. M.A. Munoz-Marquez, G.S. Parkinson, D.P. Woodruff, A. Hentz, P.L. Grande, G. Schiwietz, T.J. Wood, C. Bonet, S.P. Tear, P. Bailey, T.C.Q. Noakes, Phys. Rev. **B 72**, 075415 (2005).
17. A. Hentz, G.S. Parkinson, A. Window, P.D. Quinn, D.P. Woodruff, P.L. Grande, G. Schiwietz, P. Bailey, T.C.Q. Noakes, Phys. Rev. **B 74**, 125408 (2006).
18. G. Schiwietz, Phys. Rev. **A 42**, 296 (1990).
19. P.L. Grande and G. Schiwietz, Phys. Rev. **A 58**, 3796 (1998).
20. P.L. Grande and G. Schiwietz, URL http://www.hmi.de/people/schiwietz/casp.html.
21. C. Auth and H. Winter, Phys. Lett. **A 176**, 109 (1993).

22. N.M. Kabachnik, V.N. Kondratyev, O.V. Chumanova, Phys. Stat. Sol. (b) **145**, 103 (1988).
23. T. Okazawa, T. Nishizawa, T. Nishimura, Y. Kido, Phys. Rev. **B 75**, 033413 (2007).
24. M. Pedio, L. Becker, B. Hillert, S. D'Addato, J. Haase, Phys. Rev. **B 41**, 7462 (1990).
25. S. Nakatani, A. Saito, Y. Kuwahara, T. Takahashi, M. Aono, S. Kikuta, Jpn. J. Appl. Phys. **31**, L426 (1992).
26. J.H. McGuire and L. Weaver, Phys. Rev. **A 16**, 41 (1977).
27. P.L. Grande and G. Schiwietz, Nucl. Instrum. Methods **B 132**, 264 (1997).
28. F. Herman and S. Skillman, *Atomic Structure Calculations* (Prentice-Hall, Inc. Englewood Cliffs, New Jersey, 1963)
29. I. C. Vickridge and G. Amsel , Nucl. Instrum. Methods **B 108**, 403 (1996).
30. P.L. Grande, A. Hentz, R.P.Pezzi, I.J.R. Baumvol, G. Schiwietz, Nucl. Instrum. Methods **B 256**, 92 (2007).
31. P. Sigmund, A. Schinner, Nucl. Instrum. Methods **B 195**, 64 (2002).
32. ICRU Report 73, International Commission on Radiation Units and Measurements, J. ICRU 5, No. 1 (2005) (Oxford Univ. Press)